Cell Reports
Report

Cell PRESS
Open ACCESS

The Architecture of Yeast DNA Polymerase ζ

Yacob Gómez-Llorente,[1,3] Radhika Malik,[1,3] Rinku Jain,[1] Jayati Roy Choudhury,[2] Robert E. Johnson,[2] Louise Prakash,[2] Satya Prakash,[2] Iban Ubarretxena-Belandia,[1,*] and Aneel K. Aggarwal[1,*]

[1]Department of Structural and Chemical Biology, Icahn School of Medicine at Mount Sinai, Box 1677, 1425 Madison Avenue, New York, NY 10029, USA

[2]Department of Biochemistry and Molecular Biology, 301 University Boulevard, University of Texas Medical Branch, Galveston, TX 77755-1061, USA

[3]These authors contributed equally to this work

*Correspondence: iban.ubarretxena@mssm.edu (I.U.-B.), aneel.aggarwal@mssm.edu (A.K.A.)

http://dx.doi.org/10.1016/j.celrep.2013.08.046

SUMMARY

DNA polymerase ζ (Polζ) is specialized for the extension step of translesion DNA synthesis (TLS). Despite its central role in maintaining genome integrity, little is known about its overall architecture. Initially identified as a heterodimer of the catalytic subunit Rev3 and the accessory subunit Rev7, yeast Polζ has recently been shown to form a stable four-subunit enzyme (Polζ-d) upon the incorporation of Pol31 and Pol32, the accessory subunits of yeast Polδ. To understand the 3D architecture and assembly of Polζ and Polζ-d, we employed electron microscopy. We show here how the catalytic and accessory subunits of Polζ and Polζ-d are organized relative to each other. In particular, we show that Polζ-d has a bilobal architecture resembling the replicative polymerases and that Pol32 lies in proximity to Rev7. Collectively, our study provides views of Polζ and Polζ-d and a structural framework for understanding their roles in DNA damage bypass.

INTRODUCTION

Cellular DNA is under constant attack by external and internal agents that cause lesions and block the progression of the DNA replication machinery. Both prokaryotes and eukaryotes possess specialized translesion synthesis (TLS) DNA polymerases (Pols) that can replicate through these lesions (Prakash et al., 2005). Most of the TLS polymerases belong to the Y-family, which includes the single subunit Polη, Polι, Polκ, and Rev1 in humans (Prakash et al., 2005). Polζ is a multisubunit TLS polymerase that belongs to the B-family (Prakash et al., 2005; Sharma et al., 2013). It is specialized for the extension step of lesion bypass, whereby it is recruited to add nucleotides once another TLS polymerase has added a nucleotide opposite the lesion. The ability of Polζ to carry out synthesis downstream of DNA lesions caused by UV light and chemical mutagens (Prakash et al., 2005) is important in maintaining genome integrity and preventing cancer (Lange et al., 2011; Sharma et al., 2013). Because Polζ can extend from both correct and incorrect nucleotides opposite from DNA lesions, it also contributes to mutagenic TLS.

Although Polζ was discovered >40 years ago (Lemontt, 1971), there is still little or no structural understanding of how this TLS polymerase is organized. Polζ from *S. cerevisiae* was initially identified as a heterodimer consisting of the subunits Rev3 and Rev7 (Nelson et al., 1996). Rev3 is the catalytic subunit that belongs to the same B-family of Pols as Pol1, Pol2, and Pol3, the catalytic subunits of the high-fidelity eukaryotic replicative Polα, Polε, and Polδ, respectively (Johansson and Macneill, 2010; Johnson and O'Donnell, 2005). During replication, Polα primes the Okazaki fragments on the lagging DNA strand, which are then elongated by Polδ. Polε is believed to be the leading-strand DNA polymerase (Nick McElhinny et al., 2008). Besides the catalytic subunits, these high-fidelity polymerases in yeast also contain accessory subunits: Pol12, Pri1, and Pri2 in Polα; Dpb2, Dpb3, and Dpb4 in Polε; and Pol31 and Pol32 in Polδ (Johansson and Macneill, 2010; Johnson and O'Donnell, 2005). In mice, disruption of the Rev3 subunit of Polζ causes embryonic lethality (Prakash et al., 2005; Sharma et al., 2013). The Rev3 sequence differs from that of Pol1, Pol2, and Pol3 in containing a large insert that is the site of Rev7 binding (Figure 1A). Rev7 both stabilizes and increases the activity of Polζ. Surprisingly, Polζ has been found recently to associate with Pol31 and Pol32, the accessory subunits of Polδ (Johnson et al., 2012; Makarova et al., 2012). A stable four-subunit Rev3/Rev7/Pol31/Pol32 complex can be purified from yeast, which we refer to as Polζ-d to distinguish it from the traditional Polζ heterodimer (Johnson et al., 2012). Importantly, the Pol31 and Pol32 subunits have been shown to be essential for Polζ function in vivo, and in vitro they increase the catalytic activity of Polζ between 3-fold and 10-fold (depending on the lesion) (Johnson et al., 2012; Makarova et al., 2012). The Pol31/Pol32 subcomplex associates with Polζ via an interaction between the Rev3 C-terminal domain (CTD) and Pol31 (Baranovskiy et al., 2012; Johnson et al., 2012; Makarova et al., 2012). The Rev3 CTD contains two cysteine-rich metal-binding motifs, CysA and CysB, analogous to the motifs at the C termini of Pol1, Pol2, and Pol3. Thus, in subunit composition

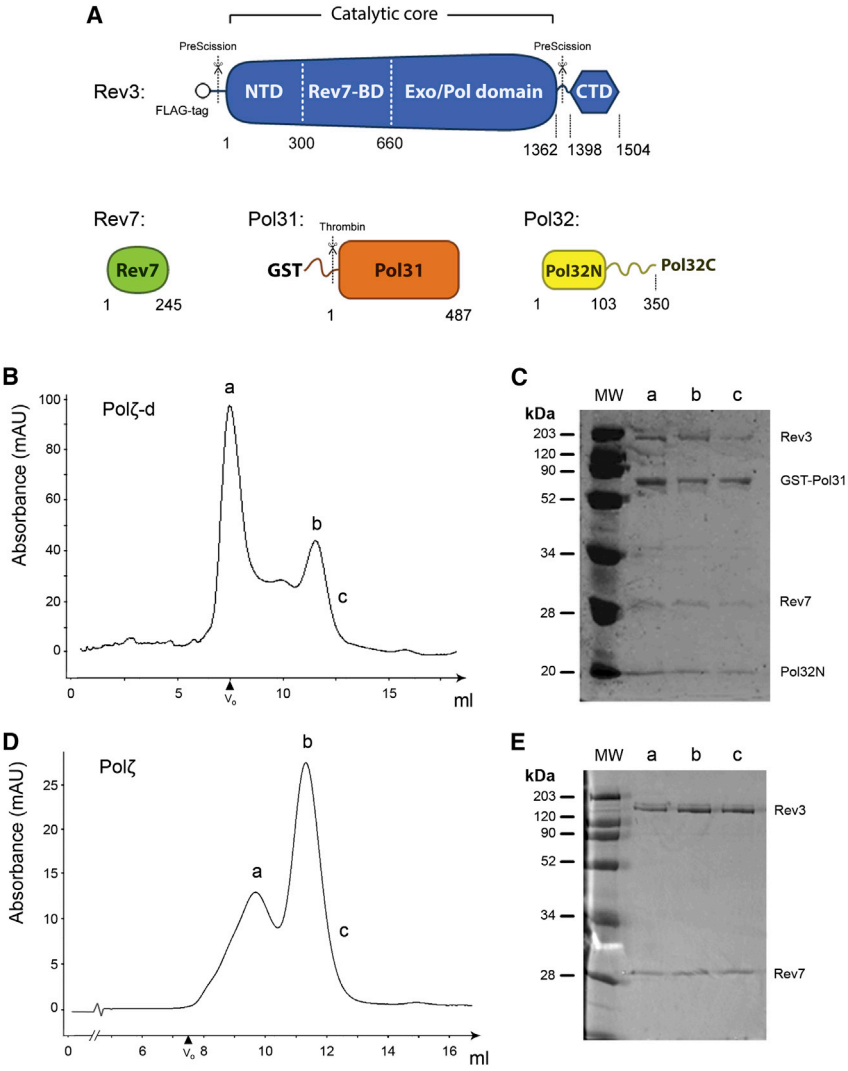

Figure 1. Purification of Polζ and Polζ-d Complexes

(A) Scheme of the proteins and domains of the Polζ and Polζ-d complexes used in this study. Numbers indicate the delimiting residues. The Rev3 catalytic core is composed of the N-terminal domain (NTD), the Rev7 binding domain (Rev7-BD), and the Exo/Pol domain. The Rev3 C-terminal domain (CTD) is joined to the catalytic core by a flexible region. Pol32N is composed of the first 103 N-terminal amino acid residues of Pol32. "PreScission" and "Thrombin" indicate protease cleavage sites.

(B) Gel filtration elution profile of Polζ-d over a Superdex 200 10/300 size exclusion column. The exclusion volume at 7.5 ml is indicated as V_o. The first and second peaks of the chromatogram are labeled as "a" and "b," whereas "c" indicates the slope of the second peak.

(C) SDS-PAGE analysis and Coomassie blue staining of this peak reveals that Polζ-d is a stable complex of the subunits Rev3:Rev7:Pol31-GST:Pol32N.

(D) Gel filtration elution profile of Polζ over a Superdex 200 10/300 size exclusion column. Peaks are labeled as described in (B).

(E) The SDS-PAGE analysis of this peak shows that Polζ forms a stable Rev3:Rev7 complex. Aliquots of the top fractions of peaks "b" were used for single-particle EM analysis for both samples.

and structural complexity, Polζ-d resembles the high-fidelity replicative Pols α, ε, and δ. The fact that it shares the same accessory subunits (Pol31 and Pol32) as Polδ raises questions as to how the activities of the two polymerases are coordinated during lesion bypass.

Current structural information on Polζ (or Polζ-d) is limited to structures of human Rev7 in complex with a short peptide (residues 1,875–1,895) from human Rev3 and a structure of the human counterpart of Pol31 (p50) in complex with the N-terminal domain of Pol32 (p66N) (Baranovskiy et al., 2008; Hara et al., 2010). To understand how Polζ and Polζ-d are assembled into functional DNA polymerases, we undertook electron microscopy (EM) analyses of the two complexes. Here, we present 3D models of yeast Polζ-d and Polζ, showing how the catalytic and accessory subunits are organized relative to each other. We show that Polζ-d has a bilobal architecture resembling the high fidelity replicative Pols, and that Pol32 lies in close proximity to Rev7. We discuss the implications of our findings for the role of Polζ in DNA damage bypass.

RESULTS

Purification and EM Analysis of Polζ-d and Polζ Complexes

To purify the four-subunit Polζ-d complex, we cotransformed plasmids expressing FLAG-tagged Rev3 (residues 1–1,504), Rev7 (residues 1–245), glutathione S-transferase (GST)-tagged Pol31 (residues 1–487), and Pol32N (residues 1–103) in *S. cerevisiae* cells (Figure 1A). The FLAG and GST tags were engineered to be cleaved with PreScission and thrombin protease, respectively, and Pol32N was designed to express only the N-terminal domain of Pol32 (residues 1–103) that interacts with Pol31. The unstructured C-terminal tail of Pol32 (residues 104–350) that contains a proliferating cell nuclear antigen (PCNA) interaction motif was omitted from the construct. The Polζ-d heterotetramer was first purified over a glutathione Sepharose column and then over an anti-FLAG agarose column. The FLAG and GST tags were not cleaved and the complex was concentrated and further purified over a Superdex-200 gel filtration column. SDS-PAGE analysis of peak "b" fraction indicated a complex consisting of Rev3, Rev7, Pol31, and Pol32N (Figures 1B and 1C). To prepare the Polζ heterodimer (Rev3/Rev7) for EM analysis, we separated it from partially purified Polζ-d. We adopted this procedure because expression of Rev3/Rev7 in the absence of Pol31/Pol32 is poor and the complex tends to aggregate. Thus, following the partial purification of Polζ-d over the glutathione Sepharose column (described above), ion exchange chromatography was used to separate the Rev3/Rev7 heterodimer from the

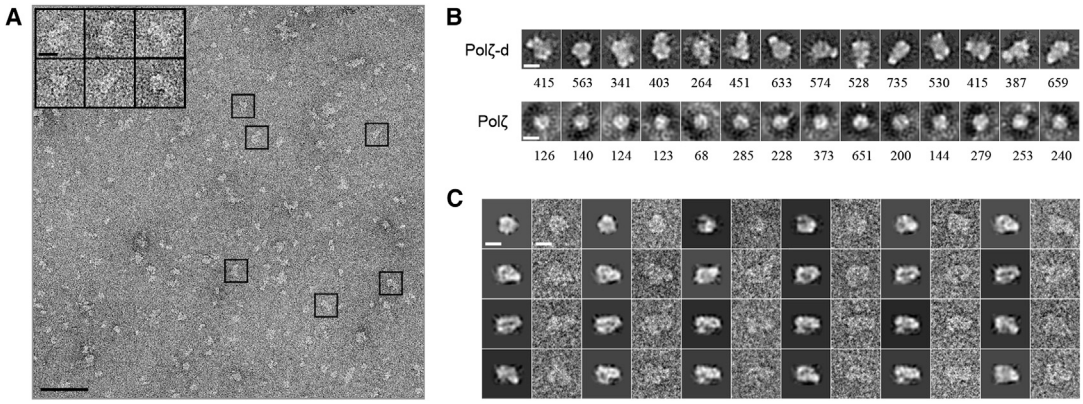

Figure 2. EM and Image Processing

(A) EM field view of negatively stained Polζ-d. Representative particle images are boxed. Scale bars indicate 50 nm in the EM field and 100 Å in the boxed particles.

(B) Maximum likelihood representative classes obtained during the iterative rounds of two-dimensional processing and classification of the raw particle images of the Polζ-d heterotetramer and the Polζ heterodimer. The number of particles included in each class is shown below every image. Masks were omitted in this analysis. Scale bars represent 100 Å.

(C) Comparison between projections of the final 3D reconstruction of Polζ-d and raw single-particle images. Every couple of images corresponds to a projection of the masked volume (the first image) and a corresponding single-particle image (the second image). Scale bars represent 100 Å.

See also Figures S1 and S2.

Pol31/Pol32N subcomplex. The Rev3/Rev7 heterodimer was then further purified over a Superdex-200 gel filtration column (Figures 1D and 1E).

Gel-filtered samples of Polζ-d and Polζ were used to prepare the EM grids. Due to the relatively small size of both Polζ-d and Polζ, we imaged the specimens embedded in negative stain to ensure sufficient contrast (Ohi et al., 2004). Figure 2A displays a representative field view of negatively stained Polζ-d showing abundant elongated particles. Approximately 56,000 single images of Polζ-d particles and 69,000 of Polζ were automatically selected using EMAN2 (Tang et al., 2007) and then subjected to iterative rounds of reference-free classification and heterogeneity analysis using two-dimensional maximum likelihood (MLF2D) (Scheres et al., 2005). The MLF2D averages for Polζ-d revealed (Figure 2B) an elongated bilobal structure that is reminiscent of the bilobal architecture previously determined for the Pol1-Pol12 complex (Klinge et al., 2009) and presumably represent side-view projections of the Polζ-d complex rotating along its longitudinal axis. Consistent with the lower molecular weight of the Polζ heterodimer (185 kDa), the MLF2D averages for this complex revealed smaller globular particles, which correspond with projections of the larger of the two lobes observed for the Polζ-d heterotetramer. Further support for this interpretation was obtained by comparative KerDenSOM heterogeneity analysis (Pascual-Montano et al., 2001) between selected particle images of Polζ and Polζ-d masked around the large lobe (Figure S1).

As a result of our MLF2D analysis, a subset of approximately 15,000 particle images of the Polζ-d heterotetramer and 2,000 of the Polζ heterodimer were employed for 3D reconstruction and refinement using Xmipp (Scheres et al., 2008). Projections of the reconstruction of Polζ-d correspond closely with individual particle images (Figure 2C), indicating consistency between the reconstructed structure and the particle data set. Based on the 0.5 criterion of the Fourier ring correlation, the final structures of Polζ-d heterotetramer and Polζ heterodimer were determined to resolutions of 23 and 25 Å, respectively (Figure S2).

Polζ-d Has a Two-Lobe Architecture with Separate Catalytic and Regulatory Modules

The 3D reconstruction of Polζ-d was rendered at a threshold that includes a volume of 344,000 $Å^3$, corresponding to a molecular weight (determined using an average protein density of 0.856 $Da/Å^3$; Fischer et al., 2004) of ~298 kDa, in agreement with the mass of the Polζ-d heterotetramer. The EM map revealed an elongated bilobal structure, in which two "stems" at the back of the structure connect the small upper lobe with the large lower lobe (Figure 3B, right panel; stems labeled as green circles A and B). There is also a prominent "protrusion" at the front of the small lobe that does not connect with the large one (labeled as a green circle C in the right panel of Figure 3B). The overall dimensions of the large lobe in Polζ-d are consistent with the molecular weight of Rev3 (173 kDa), while the small lobe has a size consistent with the combined mass of Rev7, Pol31, and Pol32N (total mass of 122 kDa). Due to the lower molecular weight of Polζ and the significantly lower number of particles used for its 3D reconstruction, the EM map of Polζ was of lower quality relative to that of Polζ-d. However, the density features shared by Polζ-d and Polζ (Figure 3B) confirm that the large lobe corresponds to the catalytic subunit Rev3. The density region corresponding to the protrusion at the front of Polζ-d heterotetramer is also apparent in the Polζ heterodimer, indicating that it likely represents Rev7. Consistent with the absence of Pol31 and Pol32 subunits in the Polζ heterodimer, the major part of the density in the small lobe of the Polζ-d heterotetramer is missing in the Polζ heterodimer.

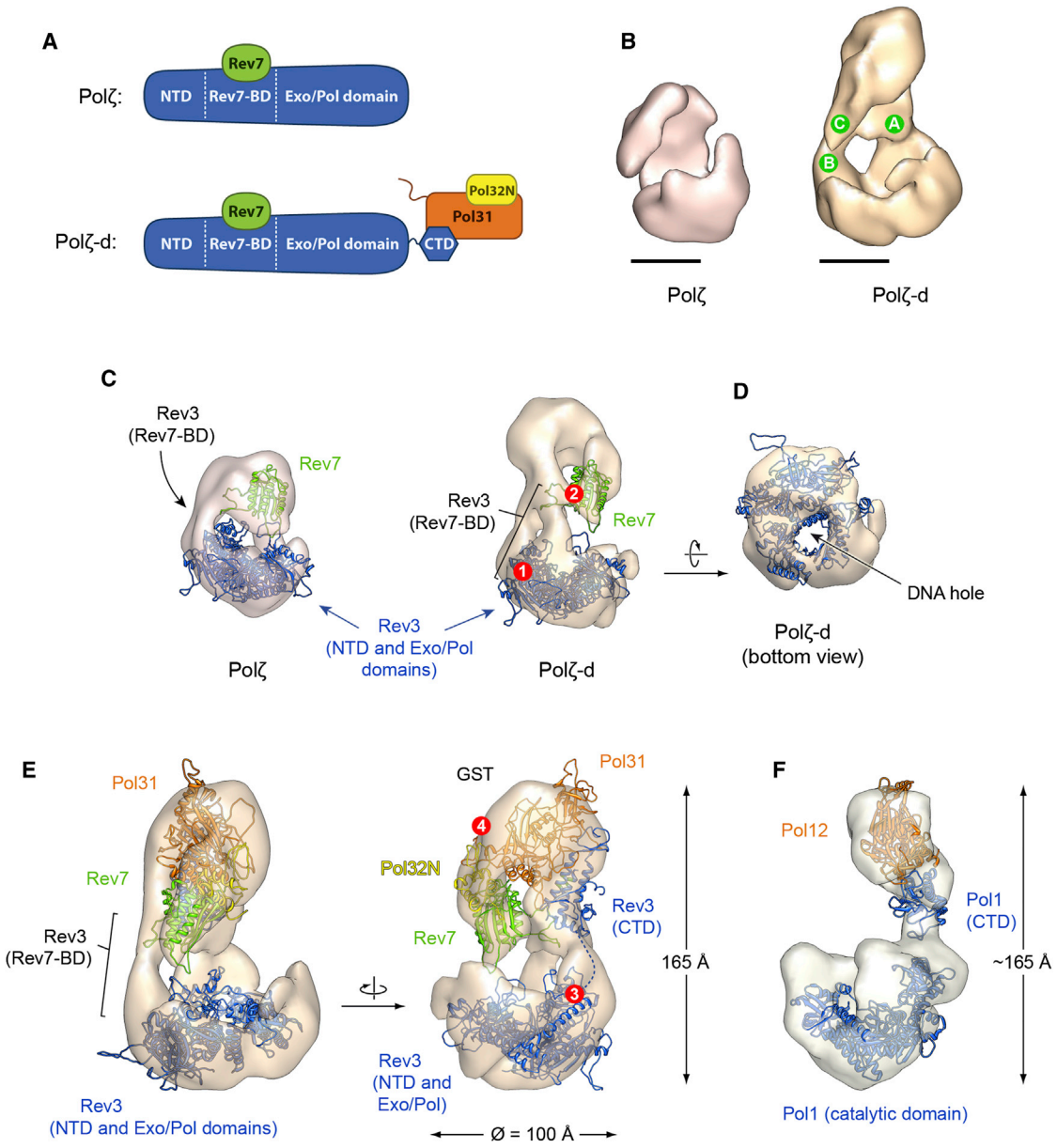

Figure 3. Structures of Polζ and Polζ-d

(A) Schema depicting the modeled regions of the different subunits of Polζ and Polζ-d.

(B) Front views of the EM reconstructions of Polζ and Polζ-d. Consecutive letters A, B, and C inside green circles mark the two stems that separate the big and small lobes and the protrusion extending from the small lobe. Scale bars represent 50 Å.

(C) Fitting of the modeled domains of Rev3 catalytic core (in blue; residues 1–300 and 660–1,362) and Rev7 (in green) into the EM maps. Both maps are rotated 90° along the z axis relative to the orientations in B. Residues flanking Rev7-BD (330 and 660, labeled with a red circle #1) are located in proximity to the assigned density of Rev7-BD. The β strands of Rev7 responsible of the interactions with Rev3 (red circle #2) are facing the Rev7-BD assigned density.

(D) Bottom view of the Polζ-d EM map, showing a hole in the density that matches the DNA hole of Rev3.

(E) Fitting of the four subunits into the EM map of the Polζ-d heterotetramer. The height of Polζ-d was measured as 165 Å. The residue 1362 of Rev3 is labeled (red circle #3), and the location of the 32 next amino acid residues that separate the CTD (residues 1,398–1,504) of the catalytic core is represented by a dashed line. The density assigned to GST is in proximity to the N-term residues of Pol31 (red circle #4).

(F) EM structure and subunit architecture of Polα in a similar orientation to our reconstruction (Klinge et al., 2009).

Homologous Pol31 and Pol12 (PDB ID 3FLO) and Rev3 and Pol1 (PDB ID 2VWJ) are depicted in (E) and (F) using identical colors. Both Polζ and Polα share a similar architecture with comparable dimensions. See also Figures S3, S4, and Movie S1.

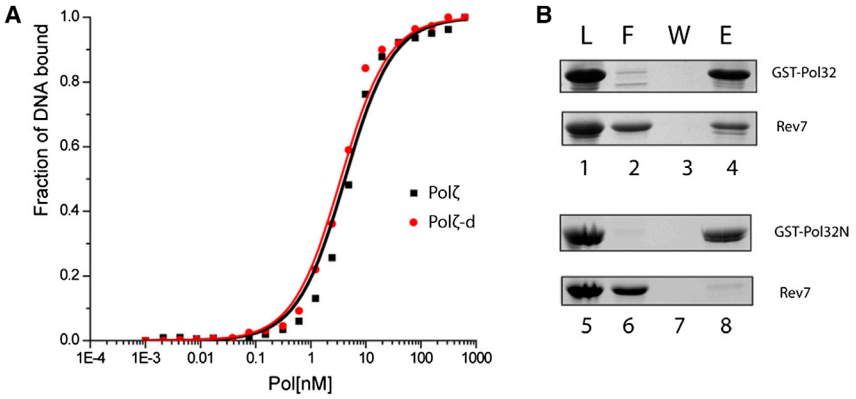

Figure 4. Biochemical Assays

(A) DNA binding activity of Polζ and Polζ-d. Binding of Polζ-d and Polζ to a 40/45 duplex DNA as monitored by changes in anisotropy during the titration. Fitting of the data yields a K_d of 3.5 ± 0.25 nM for the Polζ-d heterotetramer (red line) and a K_d of 4.2 ± 0.40 nM for the Polζ heterodimer (black line). The 6-FAM (6-carboxyfluorescein)-labeled oligonucleotides were excited at 490 nm and the resulting emission was passed through a 520 nm cutoff filter on a Beacon 2000 fluorescence polarization system. The DNA concentration was fixed at 2 nM. Protein concentration was varied from 10 pM to 625 nM.

(B) Physical interaction of Rev7 with Pol32 and Pol32N. Glutathione Sepharose bead-bound Pol32 (lanes 1–4) or Pol32N (lanes 5–8) was mixed with Rev7 and pull-down assays were done as described in Experimental Procedures. Fractions load (L, lanes 1 and 5), flow through (F, 2 and 6), wash (W, 3 and 7), and elution (E, 4 and 8) were resolved on a 15% denaturing polyacrylamide gel, followed by Coomassie blue R-250 staining. Rev7 binds to full-length Pol32, but not to the C-terminally truncated Pol32 (Pol32N). See also Figure S3 and Movie S1.

A Structural Model of Polζ-d

In order to produce a structural model of yeast Polζ-d consistent with our 3D reconstruction, we manually fitted homology models of all the subunits to match the corresponding regions of the EM map (Movie S1). To guide the placement and orientation of the subunits in the map, we used constraints derived from the comparison of the EM maps of Polζ-d and Polζ, complemented with additional constraints derived from published structural and biochemical data. We employed comparative protein structure modeling with the program Modeler (Fiser and Sali, 2003) to build homology models for yeast Rev3, Rev7, Pol31, and Pol32N. The modeled regions of the different subunits are schematized in Figure 3A. The structure of Pol3 catalytic core of yeast Polδ (Swan et al., 2009) served as a template for the catalytic core of yeast Rev3. The Rev3 CTD was modeled on the basis of the structure of yeast Pol1 CTD in complex with Pol12 (Klinge et al., 2009). In addition, the crystal structures of human Rev7 (Hara et al., 2010) and the p50-p66N heterodimer (Baranovskiy et al., 2008) served as templates to build the models of yeast Rev7 and Pol31-Pol32N, respectively.

The catalytic core of yeast Rev3 is much larger than the Rev7 subunit and could fit with a high cross correlation (CC) coefficient of 0.86 into the large lobe of Polζ-d (Figure 3C, right panel). The orientation of the catalytic core was inferred by matching a characteristic "DNA hole," also observed in the center of the structure of Pol3, with the only hole at the bottom of the large lobe of the EM map (Figure 3D). Consistently, the Rev3 catalytic core also fitted well and with the same orientation into the corresponding density in the Polζ heterodimer (Figure 3C, left panel). Rev7 fitted (CC coefficient = 0.81) into the density region suspended over Rev3 in both the Polζ-d heterotetramer and the Polζ homodimer.

The crystal structure of only a short peptide region (21 amino acids) from human Rev3, which interacts with Rev7, has been elucidated (Hara et al., 2010). Due to the lack of an appropriate structural template, we could not model the corresponding Rev7-interacting region of yeast Rev3 (residues 300–660) in Polζ and Polζ-d EM models. However, the orientation of Rev7 in our model positions the Rev3 binding site in Rev7 (red circle 2 in Figure 3C) ~50 Å away from residues 299 and 661 in Rev3 (red circle 1 in Figure 3C), in the direction of the first stem (labeled as green circle B in Figure 3B) connecting the large lobe with the small lobe in the Polζ-d EM map. We suggest that this density along the first stem corresponds to the unmodeled insert in Rev3 (residues 300–660) that connects to Rev7. On the basis of recent biochemical studies, the Pol31/Pol32 subcomplex associates with Rev3 via a direct interaction between the Rev3 CTD and Pol31. We modeled the Pol31/Pol32 complex based on the crystal structure of p50/p66N complex (Baranovskiy et al., 2008), the human counterparts of Pol31 and Pol32, and the interaction between Rev3 CTD and Pol31 was modeled on the crystal structure of Pol1 CTD/Pol12 complex (Klinge et al., 2009). The modeled Pol31-Pol32-CTD structure accounts for the major portion of the EM density (CC coefficient = 0.87) in the small lobe of Polζ-d (Figure 3E). The Rev3 CTD region of Rev3 connects to the catalytic core via a 36-amino-acid-long linker, beginning at amino acid 1,362 (red circle 3 in Figure 3E). We suggest that this unmodeled linker corresponds to the second stem (labeled as green circle A in Figure 3B) of density connecting the upper lobe with the larger lower lobe in the Polζ-d EM map.

Taken together, the structural model of Polζ-d shown in Figure 3 accounts for a majority of the EM density of the 3D reconstruction of Polζ-d (CC coefficient = 0.86). The model suggests a bilobal architecture for Polζ-d with separate catalytic and regulatory modules. The accessory subunits Rev7, Pol31, and Pol32 form the regulatory module that connects to the catalytic subunit Rev3 at two different sites via interaction with Rev7 and Pol31, respectively. The Pol31/Pol32 subunits hover above the Rev3 catalytic core, raising the possibility that they may interact with the DNA (Figure S3).

Interactions with the DNA

To test whether the Pol31/Pol32 subunits in Polζ-d increase the affinity of Polζ for DNA, we compared the binding of Polζ-d and Polζ to a fluorescein-labeled 40 nt/45 nt primer/template using fluorescence anisotropy. The length of the primer/template was based on the Polζ-d structural model, as the number of nucleotides required to span the catalytic (Rev3) and regulatory (Rev7/Pol31/Pol32) modules. Figure 4A shows that the Polζ

homodimer (Rev3/Rev7) and Polζ-d heterotetramer (Rev3/Rev7/Pol31/Pol32N) bind the primer/template with similar K_d of ~4 nM. Together, these data suggest that despite the proximity of Pol31 and Pol32N to the modeled DNA in the Polζ-d heterotetramer, these subunits do not contribute significantly to DNA binding.

Interactions between Rev7 and Pol32

Intriguingly, Rev7 and Pol32N are in close spatial proximity in our Polζ-d model, raising the possibility that Rev7 and Pol32 physically interact. We tested this idea via a GST pull-down assay. Briefly, GST-Pol32 and GST-Pol32N (C-terminally truncated Pol32, 1–104 aa) were bound to GST beads and individually mixed with Rev7. After incubation and extensive washing, the bead-bound proteins were eluted and resolved on a 15% denaturing polyacrylamide gel, followed by Coomassie blue staining. Indeed, Figure 4B shows that Rev7 binds to full-length Pol32, but not to the C-terminally truncated Pol32 (Pol32N).

Comparison to Polα

Despite differences in subunit composition and stoichiometry, a comparison between the EM structures of Polζ-d and high-fidelity Polα complexes (Klinge et al., 2009; Núñez-Ramírez et al., 2011) reveals a common architecture (Figure 3F). Both polymerases share a bilobal configuration with very similar dimensions along the longitudinal axis and separate catalytic and regulatory modules. In both polymerases, a short linker connects the polymerase catalytic core to its CTD and the respective B-accessory subunit, Pol31 in Polζ-d and Pol12 in Polα. In Polα structures, this linker has been suggested to be the source of flexibility between the regulatory and catalytic modules (Klinge et al., 2009). A study of the conformational heterogeneity of the Pol1-Pol12 complex, for example, using three-dimensional maximum likelihood in Fourier space (MLF3D) revealed that the CTD-Pol12 module could sample a range of positions relative to the catalytic core. Indeed, this intermodular flexibility appears to be a general property of replicative B-family polymerases. An EM 3D model of the yeast Polε holoenzyme suggests analogous flexibility between the catalytic subunit (Pol2) and the accessory subunits (Dpb2, Dpb3, and Dpb4) (Asturias et al., 2006). Also, small-angle X-ray scattering analysis of the yeast Polδ holoenzyme, which shares the Pol31-Pol32 subunits with Polζ, suggests high conformational variability of the regulatory module with respect to the catalytic domain (Jain et al., 2009). To examine the conformational heterogeneity in the Polζ-d heterotetramer, we performed the MLF3D procedure on the EM data but did not observe significant variation in the relative positions of the catalytic and regulatory modules (data not shown).

DISCUSSION

Here, we present 3D structural models of Polζ and Polζ-d based on EM imaging and single-particle reconstruction. We show that Polζ has a globular-like structure, whereas Polζ-d has an elongated bilobal architecture. The large lobe of Polζ-d can be fitted with the Rev3 catalytic core and the smaller lobe with the accessory subunits Rev7, Pol31, Pol32N, as well as Rev3 CTD. There are two stems of density connecting the lobes, which appear to derive from the insert in Rev3 (residues 300–660) that binds Rev7 and the linker connecting the catalytic core of Rev3 to the CTD/Pol31/Pol32N substructure. The extended bilobal architecture of Polζ-d is highly reminiscent of high-fidelity replicative Pols α and δ (Jain et al., 2009; Klinge et al., 2009; Núñez-Ramírez et al., 2011). One difference is that whereas the catalytic and regulatory modules in Polα and Polδ are flexibly tethered (Jain et al., 2009; Klinge et al., 2009), they seem to be more rigidly associated in Polζ-d. This may reflect the fact that two modules in Polζ-d are additionally tethered via Rev3-Rev7 interactions. In Polα, the flexibility between the modules is thought to be important in the transfer of the RNA primer from the active site of its primase Pri1/Pri2 subunits on one module to the active site of the polymerase Pol1 subunit on the other module (Núñez-Ramírez et al., 2011). In Polδ, flexibility may be important when there is a change in DNA direction as, for example, during a switch in the DNA primer from the polymerase to the exonuclease active site of Pol3 during DNA synthesis. In contrast, because there is no equivalent change in DNA direction when Polζ-d extends from DNA lesions this may partially obviate the need for intermodule flexibility of the type observed in Polα and Polδ.

Rev7 and Pol32N are in close spatial proximity in our Polζ-d model. We tested whether Rev7 and Pol32 physically interact via a GST pull-down assay. Intriguingly, Rev7 binds to full-length Pol32, but not to the C-terminally truncated Pol32 (Pol32N). From secondary structure analysis, the C-terminal residues of Pol32 (104–350) lack secondary structure but based on our Polζ-d model and pull-down assay appear capable of physically interacting with Rev7. This Rev7 and Pol32 interaction may be one reason why Pol32 is indispensable for Polζ-d complex formation. Thus, whereas Pol3, the catalytic subunit of Polδ, can form a stable complex with Pol31 in the absence of Pol32, Rev3/Rev7 is less stable without Pol32 (Johnson et al., 2012; Makarova et al., 2012).

Pol31 and Pol32 are essential for Polζ function in vivo, and in vitro they increase the catalytic activity of Polζ between 3-fold and 10-fold (Johnson et al., 2012; Makarova et al., 2012). Since Pol31 contains an oligonucleotide/oligosaccharide (OB) fold and an inactive phosphodiesterase domain it could, in principle, help to increase the affinity of Polζ for DNA (Baranovskiy et al., 2008); however, we show here that Polζ and Polζ-d bind DNA with similar K_ds. Pol31 and Pol32 greatly increase the stability of Rev3/Rev7 complex as indicated from the high resistance of Polζ-d to salt concentrations up to 1 M NaCl (Johnson et al., 2012). The increase in stability is also reflected in effects on catalysis, as kinetic analysis of Polζ and Polζ-d shows that increase in the catalytic efficiency of Polζ-d compared to Polζ is primarily due to an increase in k_{cat} value (Johnson et al., 2012).

Intriguingly, a deficiency in Rev1 confers a similar phenotype as a deficiency in Polζ, suggesting an interaction between the two proteins (Lawrence, 2004). Indeed, in vertebrates, Rev7 has been shown to physically associate the C-terminal region of Rev1 (Murakumo et al., 2001), and a number of crystal structures have provided the molecular basis of this interaction (Kikuchi et al., 2012; Wojtaszek et al., 2012). Figure S4 shows the C-terminal region of human Rev1, composed of four helices, docked against Rev7 in our yeast Polζ-d model. Notably, the

Rev1 C-terminal region extends from the Polζ-d core in an accessible position to engage other TLS polymerases in mammalian cells.

In conclusion, despite the critical role of Polζ (or Polζ-d) in eukaryotic DNA damage response, there has been little structural information on the architecture of the complex. Here, we present 3D structural models of Polζ and Polζ-d that demonstrate how the catalytic and accessory subunits are organized relative to each other for DNA damage bypass in eukaryotic cells.

EXPERIMENTAL PROCEDURES

Protein Expression and Purification

The Rev3/Rev7 complex in the absence of Pol31/Pol32 expresses poorly and tends to aggregate. To overcome this hurdle, we engineered constructs of the enzyme carrying several purification tags and specific protease sites, which would allow us to purify both Polζ-d and Polζ from the "same" preparation. Briefly, plasmids expressing FLAG-tagged Rev3 (residues 1–1,504), Rev7 (residues 1–245), GST-tagged Pol31 (1–487 residues), and Pol32N (residues 1–103) were cotransformed into yeast cells. The FLAG tag was engineered to be cleaved with the PreScission protease; the GST tag was linked to Pol31 via a 12-amino-acid-long linker containing a thrombin protease site; Rev3 included an additional PreScission protease site in between the catalytic core and the CTD domain; and Pol32N was designed to express only the N-terminal domain of Pol32 (residues 1–103) that interacts with Pol31. The Polζ-d heterotetramer was first purified over a glutathione Sepharose column and then over an anti-FLAG agarose column. The GST and FLAG tags were not cleaved and the complex was concentrated and further purified over a Superdex-200 Gel Filtration column. The FLAG tag was not removed because proteolysis with PreScission would have also removed the region corresponding to Pol31/Pol32/CTD; the GST tag was not removed because thrombin is a promiscuous protease and the presence of a cryptic thrombin cleavage site in Rev3 (residues 393–398). SDS-PAGE analysis of peak b fraction indicated a homogeneous complex of Rev3, Rev7, Pol31, and Pol32N (Figures 1B and 1C). To prepare the Polζ heterodimer (Rev3/Rev7) for EM analysis, we separated it from Polζ-d, which was first partially purified over the glutathione Sepharose column (described above), and then incubated with PreScission protease to remove the CTD domain of Rev3 together with Pol31/Pol32N. Following the PreScission protease treatment, ion exchange chromatography was used to separate the Rev3/Rev7 heterodimer from the CTD/Pol31/Pol32N subcomplex. The Rev3/Rev7 heterodimer was then further purified over a Superdex-200 gel filtration column (Figures 1D and 1E).

DNA Binding Experiments

DNA binding experiments were performed with a 6-FAM (6-carboxyfluorescein)-labeled 45-mer/40-mer template/primer (2 nM) on a Panvera Beacon 2000 fluorescence polarization system, with increasing concentrations of Polζ-d and Polζ complexes (10 pM to 625 nM).

Physical Interaction of Rev7 with Pol32 and Pol32N

GST beads-bound Pol32 or Pol32N were individually mixed with Rev7. The beads were spun down and washed and the bound proteins eluted with an SDS buffer.

Electron Microscopy and 3D Reconstruction

Negatively stained Polζ-d and Polζ were imaged on a Jeol 2100F FEG transmission electron microscope at 200 kV under low-dose conditions, using a 2,000 × 2,000 pixel CCD Tietz camera at the equivalent calibrated magnification of 63,450$_\times$ and −1.5 μm defocus. Particle images of Polζ-d and Polζ were automatically selected using EMAN2 (Tang et al., 2007) and then subjected to iterative rounds of reference-free classification and heterogeneity analysis using MLF2D (Scheres et al., 2005). 3D reconstruction was carried out using the software Xmipp (Scheres et al., 2008). Fitting, visualization, and 3D image generation were performed using UCSF Chimera (Goddard et al., 2007).

Modeling and Protein Interactions

The homology models for yeast Rev3, Rev7, Pol31, and Pol32 were built by comparative protein structure modeling. The approximate location and orientation of the DNA were inferred by comparison with the DNA-Pol3 complex of the DNA polymerase Polδ from yeast (Protein Data Bank [PDB] ID 3IAY).

For further details, please refer to the Extended Experimental Procedures.

ACCESSION NUMBERS

The EM map of Polζ-d has been deposited in the Electron Microscopy Data Bank (http://www.ebi.ac.uk/pdbe/emdb/) under accession number EMD-2409.

SUPPLEMENTAL INFORMATION

Supplemental Information includes Extended Experimental Procedures, four figures, and one movie and can be found with this article online at http://dx.doi.org/10.1016/j.celrep.2013.08.046.

ACKNOWLEDGMENTS

Access to electron microscopy instrumentation was provided by the New York Structural Biology Center, a STAR center supported by the New York State Office of Science, Technology, and Academic Research. Computing resources needed for this work were provided in part by the scientific computing facility of the Icahn School of Medicine at Mount Sinai. L.P. was supported by grant CA107650 from the National Institutes of Health.

Received: May 7, 2013
Revised: July 11, 2013
Accepted: August 29, 2013
Published: October 10, 2013

REFERENCES

Asturias, F.J., Cheung, I.K., Sabouri, N., Chilkova, O., Wepplo, D., and Johansson, E. (2006). Structure of Saccharomyces cerevisiae DNA polymerase epsilon by cryo-electron microscopy. Nat. Struct. Mol. Biol. *13*, 35–43.

Baranovskiy, A.G., Babayeva, N.D., Liston, V.G., Rogozin, I.B., Koonin, E.V., Pavlov, Y.I., Vassylyev, D.G., and Tahirov, T.H. (2008). X-ray structure of the complex of regulatory subunits of human DNA polymerase delta. Cell Cycle *7*, 3026–3036.

Baranovskiy, A.G., Lada, A.G., Siebler, H.M., Zhang, Y., Pavlov, Y.I., and Tahirov, T.H. (2012). DNA polymerase δ and ζ switch by sharing accessory subunits of DNA polymerase δ. J. Biol. Chem. *287*, 17281–17287.

Fischer, H., Polikarpov, I., and Craievich, A.F. (2004). Average protein density is a molecular-weight-dependent function. Protein Sci. *13*, 2825–2828.

Fiser, A., and Sali, A. (2003). Modeller: generation and refinement of homology-based protein structure models. Methods Enzymol. *374*, 461–491.

Goddard, T.D., Huang, C.C., and Ferrin, T.E. (2007). Visualizing density maps with UCSF Chimera. J. Struct. Biol. *157*, 281–287.

Hara, K., Hashimoto, H., Murakumo, Y., Kobayashi, S., Kogame, T., Unzai, S., Akashi, S., Takeda, S., Shimizu, T., and Sato, M. (2010). Crystal structure of human REV7 in complex with a human REV3 fragment and structural implication of the interaction between DNA polymerase zeta and REV1. J. Biol. Chem. *285*, 12299–12307.

Jain, R., Hammel, M., Johnson, R.E., Prakash, L., Prakash, S., and Aggarwal, A.K. (2009). Structural insights into yeast DNA polymerase delta by small angle X-ray scattering. J. Mol. Biol. *394*, 377–382.

Johansson, E., and Macneill, S.A. (2010). The eukaryotic replicative DNA polymerases take shape. Trends Biochem. Sci. *35*, 339–347.

Johnson, A., and O'Donnell, M. (2005). Cellular DNA replicases: components and dynamics at the replication fork. Annu. Rev. Biochem. *74*, 283–315.

Johnson, R.E., Prakash, L., and Prakash, S. (2012). Pol31 and Pol32 subunits of yeast DNA polymerase δ are also essential subunits of DNA polymerase ζ. Proc. Natl. Acad. Sci. USA *109*, 12455–12460.

Kikuchi, S., Hara, K., Shimizu, T., Sato, M., and Hashimoto, H. (2012). Structural basis of recruitment of DNA polymerase ζ by interaction between REV1 and REV7 proteins. J. Biol. Chem. *287*, 33847–33852.

Klinge, S., Núñez-Ramírez, R., Llorca, O., and Pellegrini, L. (2009). 3D architecture of DNA Pol alpha reveals the functional core of multi-subunit replicative polymerases. EMBO J. *28*, 1978–1987.

Lange, S.S., Takata, K., and Wood, R.D. (2011). DNA polymerases and cancer. Nat. Rev. Cancer *11*, 96–110.

Lawrence, C.W. (2004). Cellular functions of DNA polymerase zeta and Rev1 protein. Adv. Protein Chem. *69*, 167–203.

Lemontt, J.F. (1971). Mutants of yeast defective in mutation induced by ultraviolet light. Genetics *68*, 21–33.

Makarova, A.V., Stodola, J.L., and Burgers, P.M. (2012). A four-subunit DNA polymerase ζ complex containing Pol δ accessory subunits is essential for PCNA-mediated mutagenesis. Nucleic Acids Res. *40*, 11618–11626.

Murakumo, Y., Ogura, Y., Ishii, H., Numata, S., Ichihara, M., Croce, C.M., Fishel, R., and Takahashi, M. (2001). Interactions in the error-prone postreplication repair proteins hREV1, hREV3, and hREV7. J. Biol. Chem. *276*, 35644–35651.

Nelson, J.R., Lawrence, C.W., and Hinkle, D.C. (1996). Thymine-thymine dimer bypass by yeast DNA polymerase zeta. Science *272*, 1646–1649.

Nick McElhinny, S.A., Gordenin, D.A., Stith, C.M., Burgers, P.M., and Kunkel, T.A. (2008). Division of labor at the eukaryotic replication fork. Mol. Cell *30*, 137–144.

Núñez-Ramírez, R., Klinge, S., Sauguet, L., Melero, R., Recuero-Checa, M.A., Kilkenny, M., Perera, R.L., García-Alvarez, B., Hall, R.J., Nogales, E., et al. (2011). Flexible tethering of primase and DNA Pol α in the eukaryotic primosome. Nucleic Acids Res. *39*, 8187–8199.

Ohi, M., Li, Y., Cheng, Y., and Walz, T. (2004). Negative staining and image classification - powerful tools in modern electron microscopy. Biol. Proced. Online *6*, 23–34.

Pascual-Montano, A., Donate, L.E., Valle, M., Bárcena, M., Pascual-Marqui, R.D., and Carazo, J.M. (2001). A novel neural network technique for analysis and classification of EM single-particle images. J. Struct. Biol. *133*, 233–245.

Prakash, S., Johnson, R.E., and Prakash, L. (2005). Eukaryotic translesion synthesis DNA polymerases: specificity of structure and function. Annu. Rev. Biochem. *74*, 317–353.

Scheres, S.H., Valle, M., Nuñez, R., Sorzano, C.O., Marabini, R., Herman, G.T., and Carazo, J.M. (2005). Maximum-likelihood multi-reference refinement for electron microscopy images. J. Mol. Biol. *348*, 139–149.

Scheres, S.H., Núñez-Ramírez, R., Sorzano, C.O., Carazo, J.M., and Marabini, R. (2008). Image processing for electron microscopy single-particle analysis using XMIPP. Nat. Protoc. *3*, 977–990.

Sharma, S., Helchowski, C.M., and Canman, C.E. (2013). The roles of DNA polymerase ζ and the Y family DNA polymerases in promoting or preventing genome instability. Mutat. Res. *743-744*, 97–110.

Swan, M.K., Johnson, R.E., Prakash, L., Prakash, S., and Aggarwal, A.K. (2009). Structural basis of high-fidelity DNA synthesis by yeast DNA polymerase delta. Nat. Struct. Mol. Biol. *16*, 979–986.

Tang, G., Peng, L., Baldwin, P.R., Mann, D.S., Jiang, W., Rees, I., and Ludtke, S.J. (2007). EMAN2: an extensible image processing suite for electron microscopy. J. Struct. Biol. *157*, 38–46.

Wojtaszek, J., Lee, C.J., D'Souza, S., Minesinger, B., Kim, H., D'Andrea, A.D., Walker, G.C., and Zhou, P. (2012). Structural basis of Rev1-mediated assembly of a quaternary vertebrate translesion polymerase complex consisting of Rev1, heterodimeric polymerase (Pol) ζ, and Pol κ. J. Biol. Chem. *287*, 33836–33846.